European Journal of Computational Mechanics, 2013
Vol. 22, Nos. 5–6, 304–329, http://dx.doi.org/10.1080/17797179.2013.849910

Taylor & Francis
Taylor & Francis Group

Reconstruction of an additive space- and time-dependent heat source

A. Hazanee and D. Lesnic*

Department of Applied Mathematics, University of Leeds, Leeds LS2 9JT, UK

In this paper, we consider the inverse problem of simultaneous determination of an additive space- and time-dependent heat source together with the temperature in the heat equation, with Dirichlet boundary conditions and two over-determination conditions. These latter ones consist of a specified temperature measurement at an internal point and a time-average temperature condition. The mathematical problem is linear but ill-posed since the continuous dependence on the input data is violated. In discretised form, the problem reduces to solving an ill-conditioned system of linear equations. We investigate the performances of several regularisation methods and examine their stability with respect to noise in the input data. The boundary element method combined with either the truncated singular value decomposition, or the Tikhonov regularisation, using various methods for choosing regularisation parameters, e.g. the *L*-curve method, the generalised cross-validation criterion, the discrepancy principle and the *L*-surface method, are utilised in order to obtain accurate and stable numerical solutions.

Keywords: boundary element method; heat equation; heat source; inverse problem; regularisation; singular value decomposition

1. Introduction

Consider, for example, a practical situation in which a fertiliser from a field is carried into a stream by rain in the form of run-off which in turn affects aquatic life. Then in this application of water pollution, the unknown inhomogeneous source forcing term in the governing equation model needs to be determined.

Inverse source problems for the heat equation have recently attracted considerable interest, see (Ahmadabadi, Arab, & Maalek-Ghaini, 2009; Hazanee, Ismailov, Lesnic, & Kerimov, 2013; Ismailov, Kanca, & Lesnic, 2011; Xiong, Yan, & Wang, 2011; Yang, Dehghan, Yua, & Luoa, 2011; Yan, Yang, & Fu, 2009) to name just a few. These studies have sought a coefficient source function depending on either space- or time-dependent variables using various techniques. Aside from this, in recent years, the inverse heat source problem in multi-variables has been investigated by Yang, Yu, Luo, and Deng (2012) who determined an unknown source function, which depends on both space and time variables, from finite measurement data.

The objective of this study is to determine inverse heat source functions depending on both space and time, but which are additively separated into two unknown coefficient source functions, namely, one component dependent on space and another component dependent on time. The additional measurement/overspecified conditions are one temperature measurement, as a function of time, at one specified interior location and a time-average temperature throughout the space solution domain. The unique

*Corresponding author. Email: amt5ld@maths.leeds.ac.uk

solvability of this inverse source problem was already established by Ivanchov (Ivanchov, 2001) and it is the objective of this paper to obtain a stable numerical solution of this still ill-posed problem.

Since the governing partial differential equation is the linear heat equation with constant coefficients, the preferred method of discretisation is the boundary element method (BEM). Through the employment of the Green's formula and fundamental solution, the BEM naturally reduces the dimensionality of the problem by one, although domain integrals are still present due to the initial condition and the heat source.

Even though the inverse heat source problem is uniquely solvable, it is still ill-posed since small errors which inherently occur in any practical measurement cause largely oscillating solutions. To overcome this instability, regularisation such as the truncated singular value decomposition (TSVD), or the Tikhonov regularisation method needs to be employed. Prior to this study, the authors have experienced the use of these standard methods for solving related inverse source problems, see, for example (Farcas & Lesnic, 2006; Hazanee et al., 2013; Hazanee & Lesnic, 2013). An issue here is how to select an appropriate regularisation parameter. However, there exist many methods such as the L-curve method, the generalised cross-validation (GCV) criterion and the discrepancy principle which are all popular and successful methods for choosing the regularisation parameter. Moreover, the selection of multiple regularisation parameters based on the L-hypersurface (the L-surface for two parameters), has been introduced in (Belge, Kilmer, & Miller, 2002), as a natural extension of the L-curve method used for the selection of a single regularisation parameter. Hence, in this paper, the BEM is combined with either the TSVD or the Tikhonov regularisation in order to obtain stable solutions. Moreover, the L-curve method, the GCV criterion, the discrepancy principle and the L-surface criterion are employed for the selection of the regularisation parameter(s).

This paper is organised as follows. In Section 2, the mathematical inverse formulation is described and the numerical discretisation of the problem using the BEM is presented in Section 3. The TSVD and the Tikhonov regularisation are described in Section 4, as procedures for overcoming the instability of the solution. Finally, Sections 5 and 6 discuss the numerical results and highlight the conclusions of this research.

2. Mathematical formulation

Let $L > 0$ and $T > 0$ be fixed numbers and consider the inverse problem of finding the temperature $u(x,t) \in H^{2+\gamma,1+\gamma/2}(\overline{D}_T)$, with $\gamma \in (0, 1)$, and $D_T := (0, L) \times (0, T)$, the time-dependent heat source $r(t) \in H^{\gamma/2}[0, T]$ and the space-dependent heat source $s(x) \in H^{\gamma}[0, L]$ satisfying the heat conduction equation

$$u_t = u_{xx} + r(t)f(x,t) + s(x)g(x,t) + h(x,t), \quad (x,t) \in D_T, \tag{1}$$

subject to the initial condition

$$u(x,0) = \varphi(x), \quad x \in [0,L], \tag{2}$$

the Dirichlet boundary conditions

$$u(0,t) = \mu_0(t), \quad u(L,t) = \mu_L(t), \quad t \in [0,T], \tag{3}$$

and the over-determination conditions

$$u(X_0,t)=\chi(t),\quad t\in[0,T], \tag{4}$$

$$\int_0^T u(x,t)\,dt=\psi(x),\quad x\in[0,L], \tag{5}$$

$$s(X_0)=S_0, \tag{6}$$

when $f(x,t)$, $g(x,t)$, $h(x,t)$, $\varphi(x)$, $\mu_0(t)$, $\mu_L(t)$, $\chi(t)$, $\psi(x)$ are given functions, X_0 is a given sensor location within the interval $(0, L)$, and S_0 is a given value of the source function s at the given point X_0. In the above, the Hölder spaces of functions are defined in Ladyženskaja, Solonnikov, and Ural'ceva (1968, p.7).

One can remark that the time-overage temperature measurement (5) represents a non-local condition/measurement. It is convenient to use in practical situations where a local measurement of the temperature at a fixed time $\overline{T}\in(0,T]$, namely,

$$u(x,\overline{T})=:\psi_{\overline{T}}(x),\quad x\in[0,L]$$

contains a large amount of noise. This may be due to harsh external conditions, or to the fact that many space measurements can, in fact, never be recorded at a fixed instant instantaneously. If this is the case, one can have a selection of such large noise local temperature measurements, but which on average produce a less noisy non-local measurement (5).

The individual separate cases concerning the identification of a single time-dependent heat source $r(t)$, when $s(x)$ is known, or the identification of a single space-dependent heat source $s(x)$, when $r(t)$ is known, have been theoretically investigated in Prilepko and Solov'ev (1988) and Prilepko and Tkachenko (2003), respectively.

For the inverse problem (1)–(6) we have the following local unique solvability result.

Theorem 1. (Ivanchov, 2001) *Assume that the following conditions are satisfied:*

(1) $\varphi(x),\psi(x)\in H^{2+\gamma}[0,L],\mu_0(t),\mu_L(t),\chi(t)\in H^{1+\gamma/2}[0,T],h(x,t)\in H^{\gamma,\gamma/2}(\overline{D_T})$, f independent of t and $f(x)\in H^{\gamma}[0,L]$, g independent of x and $g(t)\in H^{\gamma/2}[0,T]$;

(2) $f(X_0)\neq 0$, $\int_0^T g(t)\,dt\neq 0$, $\frac{g(t)}{\int_0^T g(\tau)\,d\tau}\geq 0$, $\forall t\in[0,T]$;

(3) $\varphi(0)=\mu_0(0)$, $\varphi(L)=\mu_L(0)$, $\varphi(X_0)=\chi(0)$, $\int_0^T\chi(t)\,dt=\psi(X_0)$, $\psi(0)=\int_0^T\mu_0(t)\,dt$, $\psi(L)=\int_0^T\mu_L(t)\,dt$.

Then for sufficiently small $T>0$ there exists a unique solution of the inverse problem (1)–(6).

Note that condition (6) was omitted in (Ivanchov, 2001), but it should be included in order to avoid the following non-uniqueness counterexample.

Counter Example 1 (non-uniqueness of solution of problem (1)–(5))

For an arbitrary constant c, the identity

$$r(t)f(x)+s(x)g(t)=(r(t)+cg(t))f(x)+(s(x)-cf(x))g(t)$$

means that the heat Equation (1) is satisfied by both sets of solutions ($r(t)$, $s(x)$) and ($r(t) + cg(t)$, $s(x) - cf(x)$). This shows the non-uniqueness of the solution of the incompletely formulated inverse source problem (1)–(5). According to this, Equation (6) needs to be imposed in order to specify a particular solution.

We also note that Theorem 1 holds in higher dimensions. Although the inverse problem (1)–(6) is uniquely solvable, the problem is still ill-posed because the continuous dependence on the input data (4) and (5) is violated. This instability can be seen from the following counterexample.

Counter Example 2 (instability of problem (1)–(6))

Let $L = \pi$, $X_0 = \pi/2$ and

$$u_n(x,t) = \frac{(1 - e^{-4n^2 t})\sin(2nx)}{n^{3/2}} + \frac{x(\pi - x)\sin(nt)}{n^{1/2}}, \tag{7}$$

for n positive integer. Then the initial and boundary conditions (2) and (3) are all homogeneous. The over-determination conditions (4) and (5) are given by

$$u(\frac{\pi}{2}, t) = \chi(t) = \frac{\pi^2 \sin(nt)}{4n^{1/2}}, \quad t \in [0, T], \tag{8}$$

$$\int_0^T u(x,t)\, dt = \psi(x) = \frac{\sin(2nx)}{n^{3/2}}\left[T + \frac{e^{-4n^2 T} - 1}{4n^2}\right] + \frac{x(\pi - x)(1 - \cos(nT))}{n^{3/2}},$$
$$x \in [0, \pi]. \tag{9}$$

One can observe that the input data (8) and (9) tend to zero as $n \to \infty$. We also take

$$f(x,t) = x(\pi - x), g(x,t) = 1, h(x,t) = \frac{2\sin(nt)}{n^{1/2}}, \quad s\left(\frac{\pi}{2}\right) = S_0 = 0. \tag{10}$$

One can also observe that h tends to zero as $n \to \infty$. The above input satisfies the hypotheses of Theorem 1 and therefore the inverse problem (1)–(6) is locally uniquely solvable. In fact, one can easily check that it has the unique (global) solution

$$r_n(t) = n^{1/2}\cos(nt), s_n(x) = -4n^{1/2}\sin(2nx), \tag{11}$$

and $u_n(x, t)$ given by (7). However, one can observe that the solution (11) is unstable since it becomes unbounded as $n \to \infty$ in any reasonable norm. □

As in (Rundell, 1980), we believe that the stability of solution can be restored under stronger assumptions, e.g. if $\| \chi \|_{H^1[0,T]} \to 0$, $\| \psi \|_{H^2[0,L]} \to 0$ then, $\| s \|_{L^2[0,1]} \to 0$ and $\| r \|_{L^2[0,T]} \to 0$.

In the next Sections 3 and 4, we will demonstrate how to solve this inverse heat source problem (1)–(6) using a regularised BEM.

3. The boundary element method

Let us consider the fundamental solution G of the one-dimensional heat equation, namely

$$G(x,t,y,\tau)=\frac{H(t-\tau)}{\sqrt{4\pi(t-\tau)}}\exp\left(-\frac{(x-y)^2}{4(t-\tau)}\right),$$

where H is the Heaviside step function. By the means of this fundamental solution and the Green's formula, we obtain the following boundary integral equation, see e.g. (Farcas & Lesnic, 2006; Hazanee et al., 2013; Hazanee & Lesnic, 2013),

$$\begin{aligned}\eta(x)u(x,t)=&\int_0^t\left[G(x,t,\xi,\tau)\frac{\partial u}{\partial n(\xi)}(\xi,\tau)-u(\xi,\tau)\frac{\partial G}{\partial n(\xi)}(x,t,\xi,\tau)\right]_{\xi\in\{0,L\}}d\tau\\&+\int_0^L G(x,t,y,0)u(y,0)\,dy+\int_0^L\int_0^T G(x,t,y,\tau)r(\tau)f(y,\tau)\,d\tau dy\\&+\int_0^L\int_0^T G(x,t,y,\tau)s(y)g(y,\tau)\,d\tau dy\\&+\int_0^L\int_0^T G(x,t,y,\tau)h(y,\tau)\,d\tau dy,\quad (x,t)\in[0,L]\times(0,T),\end{aligned}\tag{12}$$

where $\eta(0)=\eta(L)=\frac{1}{2}$, $\eta(x)=1$ for $x\in(0,L)$ and $\underline{n}$ is the outward normal to the space boundary $\{0,L\}$, i.e. $\frac{\partial}{\partial n(\xi)}=\begin{pmatrix}-\frac{\partial}{\partial\xi} & \text{if } \xi=0\\ \frac{\partial}{\partial\xi} & \text{if } \xi=L\end{pmatrix}$. We divide the boundaries $\{0\}\times(0,T]$ and $\{L\}\times[0,T]$ into N small time-intervals $[t_{j-1},t_j]$, $j=\overline{1,N}$, with $t_j=\frac{jT}{N}, j=\overline{0,N}$, whilst the initial domain $[0,L]\times\{0\}$ is divided into N_0 small cells $[x_{k-1},x_k]$, $k=\overline{1,N_0}$ with $x_k=\frac{k}{N_0}, k=\overline{0,N_0}$. The boundary temperature u and the flux $\frac{\partial u}{\partial n}$ are assumed to be constant over each boundary element $[t_{j-1},t_j]$ and take their values at the midpoint $\tilde{t}_j=\frac{t_{j-1}+t_j}{2}$, i.e.

$$u(0,t)=u(0,\tilde{t}_j)=\mu_0(\tilde{t}_j)=:\mu_{0j},\quad u(L,t)=u(L,\tilde{t}_j)=\mu_L(\tilde{t}_j)=:\mu_{Lj},\quad t\in(t_{j-1},t_j],$$

$$\frac{\partial u}{\partial n}(0,t)=\frac{\partial u}{\partial n}(0,\tilde{t}_j)=:q_{0j},\quad \frac{\partial u}{\partial n}(L,t)=\frac{\partial u}{\partial n}(L,\tilde{t}_j)=:q_{Lj},\quad t\in(t_{j-1},t_j].$$

Similarly, the initial temperature is assumed to be constant over each cell $[x_{k-1},x_k]$ and takes its value at the midpoint $\tilde{x}_k=\frac{x_{k-1}+x_k}{2}$, i.e.

$$u(x,0)=u(\tilde{x}_k,0)=\varphi(\tilde{x}_k)=:\varphi_k,\quad x\in[x_{k-1},x_k].$$

Nevertheless, higher-order, e.g. linear boundary element approximations will be more accurate than constant boundary elements. This improvement in accuracy will be significant in higher-dimension, see e.g. (Skerget & Brebbia, 1985), but in our one-dimensional time-dependent setting the use of the constant BEM approximation was found sufficiently accurate.

With the approximations above, the integral Equation (12) can be approximated as

$$\begin{aligned}\eta(x)u(x,t)=&\sum_{j=1}^{N}\left[A_{0j}(x,t)q_{0j}+A_{Lj}(x,t)q_{Lj}-B_{0j}(x,t)\mu_{0j}-B_{Lj}(x,t)\mu_{Lj}\right]\\&+\sum_{k=1}^{N_0}C_k(x,t)\varphi_k+d_1(x,t)+d_2(x,t)+d_0(x,t),\quad (x,t)\in[0,L]\times(0,T),\end{aligned}\tag{13}$$

where the coefficients are given by

$$A_{\xi j}(x,t) = \int_{t_{j-1}}^{t_j} G(x,t,\xi,\tau)\ d\tau \quad \text{for} \quad \xi = \{0, L\}, \tag{14}$$

$$B_{\xi j}(x,t) = \int_{t_{j-1}}^{t_j} \frac{\partial G}{\partial n(\xi)}(x,t,\xi,\tau)\ d\tau \quad \text{for} \quad \xi = \{0, L\}, \tag{15}$$

$$C_k(x,t) = \int_{x_{k-1}}^{x_k} G(x,t,y,0)\ dy, \tag{16}$$

and the double integral source terms are given by

$$d_1(x,t) = \int_0^L \int_0^T G(x,t,y,\tau) r(\tau) f(y,\tau)\ d\tau dy, \tag{17}$$

$$d_2(x,t) = \int_0^L \int_0^T G(x,t,y,\tau) s(y) g(y,\tau)\ d\tau dy, \tag{18}$$

$$d_0(x,t) = \int_0^L \int_0^T G(x,t,y,\tau) h(y,\tau)\ d\tau dy. \tag{19}$$

The integrals (14)–(16) can be evaluated numerically analytically, (Farcas & Lesnic, 2006), whereas integrals (17)–(19) are calculated by applying the piecewise constant approximations to the functions $f(x, t)$, $g(x, t)$, $h(x, t)$, $r(t)$ and $s(x)$, as

$$f(x,t) = f(x,\tilde{t}_j), \quad g(x,t) = g(\tilde{x}_k,t), \quad h(x,t) = h(x,\tilde{t}_j),$$

$$r(t) = r(\tilde{t}_j) =: r_j, \quad s(x) = s(\tilde{x}_k) =: s_k,$$

where $t \in (t_{j\text{-}1}, t_j]$, $x \in (x_{k\text{-}1}, x_k]$ for $j = \overline{1,N}$, $k = \overline{1,N_0}$. Then the integrals (17)–(19) can be approximated as

$$d_1(x,t) = \int_0^T r(\tau) \int_0^L G(x,t,y,\tau)\, f(y,\tau)\ dy d\tau = \sum_{j=1}^{N} D_{1,j}(x,t) r_j,$$

$$d_2(x,t) = \int_0^L s(y) \int_0^T G(x,t,y,\tau)\ g(y,\tau)\ d\tau dy = \sum_{k=1}^{N_0} D_{2,k}(x,t) s_k,$$

$$d_0(x,t) = \int_0^T \int_0^L G(x,t,y,\tau)\ h(y,\tau)\ dy d\tau = \sum_{j=1}^{N} D_{0,j}(x,t),$$

where

$$D_{1,j}(x,t) = \int_0^L f(y,\tilde{t}_j) A_{yj}(x,t)\ dy,$$

$$D_{2,k}(x,t)=\frac{1}{2}\int_0^T g(\tilde{x}_k,t)H(t-\tau)\left[\operatorname{erf}\left(\frac{x-x_{k-1}}{2\sqrt{t-\tau}}\right)-\operatorname{erf}\left(\frac{x-x_k}{2\sqrt{t-\tau}}\right)\right]d\tau,$$

$$D_{0,j}(x,t)=\int_0^L h(y,\tilde{t}_j)A_{yj}(x,t)\,dy.$$

These integrals are evaluated using Simpson's rule for numerical integration. With these approximations, the integral Equation (13) becomes

$$\begin{aligned}\eta(x)u(x,t)=&\sum_{j=1}^{N}\left[A_{0j}(x,t)q_{0j}+A_{Lj}(x,t)q_{Lj}-B_{0j}(x,t)\mu_{0j}-B_{Lj}(x,t)\mu_{Lj}\right]\\&+\sum_{k=1}^{N_0}C_k(x,t)\varphi_k+\sum_{j=1}^{N}D_{1,j}(x,t)r_j+\sum_{k=1}^{N_0}D_{2,k}(x,t)s_k\\&+\sum_{j=1}^{N}D_{0,j}(x,t),(x,t)\in[0,L]\times(0,T).\end{aligned}\tag{20}$$

Applying the Equation (20) at the boundary nodes $(0,\tilde{t}_i)$ and $(L,\tilde{t}_i)$ for $i=\overline{1,N}$ yields the system of $2N$ linear equations

$$A\underline{q}-B\underline{\mu}+C\underline{\varphi}+D_1\underline{r}+D_2\underline{s}+\underline{d}=\underline{0},\tag{21}$$

where

$$A=\begin{bmatrix}A_{0j}(0,\tilde{t}_i) & A_{Lj}(0,\tilde{t}_i)\\ A_{0j}(L,\tilde{t}_i) & A_{Lj}(L,\tilde{t}_i)\end{bmatrix}_{2N\times 2N},\quad B=\begin{bmatrix}B_{0j}(0,\tilde{t}_i)+\frac{1}{2}\delta_{ij} & B_{Lj}(0,\tilde{t}_i)\\ B_{0j}(L,\tilde{t}_i) & B_{Lj}(L,\tilde{t}_i)+\frac{1}{2}\delta_{ij}\end{bmatrix}_{2N\times 2N},$$

$$C=\begin{bmatrix}C_k(0,\tilde{t}_i)\\ C_k(L,\tilde{t}_i)\end{bmatrix}_{2N\times N_0},\quad D_1=\begin{bmatrix}D_{1,j}(0,\tilde{t}_i)\\ D_{1,j}(L,\tilde{t}_i)\end{bmatrix}_{2N\times N},\quad D_2=\begin{bmatrix}D_{2,k}(0,\tilde{t}_i)\\ D_{2,k}(L,\tilde{t}_i)\end{bmatrix}_{2N\times N_0},$$

$$\underline{d}=\begin{bmatrix}\sum_{j=1}^{N}D_{0,j}(0,\tilde{t}_i)\\ \sum_{j=1}^{N}D_{0,j}(L,\tilde{t}_i)\end{bmatrix}_{2N},\ \underline{q}=\begin{bmatrix}q_{0j}\\ q_{Lj}\end{bmatrix}_{2N},\ \underline{\mu}=\begin{bmatrix}\mu_{0j}\\ \mu_{Lj}\end{bmatrix}_{2N},\ \underline{\varphi}=[\varphi_k]_{N_0},\ \underline{r}=[r_j]_N,\ \underline{s}=[s_k]_{N_0},$$

and δ_{ij} is the Kronecker delta symbol.

To determine $\underline{r}$ and $\underline{s}$, the conditions (4)–(6) are imposed. To impose (4), we apply the Equation (20) at the interior points $(X_0,\tilde{t}_i)$ for $i=\overline{1,N}$ giving rise to the following linear system of N equations:

$$A^I\underline{q}-B^I\underline{\mu}+C^I\underline{\varphi}+D_1^I\underline{r}+D_2^I\underline{s}+\underline{d}^I=\underline{\chi},\tag{22}$$

where

$$A^I=\begin{bmatrix}A_{0j}(X_0,\tilde{t}_i) & A_{Lj}(X_0,\tilde{t}_i)\end{bmatrix}_{N\times 2N},\quad B^I=\begin{bmatrix}B_{0j}(X_0,\tilde{t}_i) & B_{Lj}(X_0,\tilde{t}_i)\end{bmatrix}_{N\times 2N},$$

$$C^I=[C_k(X_0,\tilde{t}_i)]_{N\times N_0},\quad D_1^I=\begin{bmatrix}D_{1,j}(X_0,\tilde{t}_i)\end{bmatrix}_{N\times N},\quad D_2^I=\begin{bmatrix}D_{2,k}(X_0,\tilde{t}_i)\end{bmatrix}_{N\times N_0},$$

$$\underline{d}^I = \left[\sum_{j=1}^{N} D_{0,j}(X_0, \tilde{t}_i)\right]_N, \quad \underline{\chi} = [\chi_i]_N, \quad \text{where} \quad \chi_i := \chi(\tilde{t}_i) = u(X_0, \tilde{t}_i), i = \overline{1, N}.$$

The time-integral condition (5) is approximated by the midpoint numerical integration as follows:

$$\psi(x) = \int_0^T u(x,t)\ dt = \frac{T}{N}\sum_{i=1}^{N} u(x, \tilde{t}_i), \quad x \in [0, L].$$

Applying this equation at the midpoint $\tilde{x}_k$ for $k = \overline{1, N_0}$ gives

$$\frac{T}{N}\sum_{i=1}^{N} u(\tilde{x}_k, \tilde{t}_i) = \psi(\tilde{x}_k) = :\psi_k. \tag{23}$$

Using (20), Equation (23) yields

$$\frac{T}{N}\sum_{i=1}^{N}\left[A_i^{II}\underline{q} - B_i^{II}\underline{\mu} + C_i^{II}\underline{\varphi} + D_{1,i}^{II}\underline{r} + D_{2,i}^{II}\underline{s} + \underline{d}_i^{II}\right] = \underline{\psi}, \tag{24}$$

where

$$A_i^{II} = \left[A_{0j}(\tilde{x}_k, \tilde{t}_i) \quad A_{Lj}(\tilde{x}_k, \tilde{t}_i)\right]_{N_0 \times 2N}, \quad B_i^{II} = \left[B_{0j}(\tilde{x}_k, \tilde{t}_i) \quad B_{Lj}(\tilde{x}_k, \tilde{t}_i)\right]_{N_0 \times 2N},$$

$$C_i^{II} = [C_k(\tilde{x}_k, \tilde{t}_i)]_{N_0 \times N_0}, \quad D_{1,i}^{II} = \left[D_{1,j}(\tilde{x}_k, \tilde{t}_i)\right]_{N_0 \times N}, \quad D_{2,i}^{II} = \left[D_{2,k}(\tilde{x}_k, \tilde{t}_i)\right]_{N_0 \times N_0},$$

$$\underline{d}_i^{II} = [\sum_{j=1}^{N} D_{0,j}(\tilde{x}_k, \tilde{t}_i)]_{N_0}, \quad \underline{\psi} = [\psi_k]_{N_0}, \quad \text{where} \quad \psi_k := \psi(\tilde{x}_k), k = \overline{1, N_0}.$$

Finally, we consider the condition (6). Since we have used the space midpoint discretisation, we then approximate S_0 at the given point $X_0 \in (0, L)$ as

$$S_0 = s(X_0) \approx \frac{s(\tilde{x}_{k^*}) + s(\tilde{x}_{k^*+1})}{2}, \tag{25}$$

where k^* is the number in $\{1, \ldots, N_0 - 1\}$ which satisfies $\tilde{x}_{k^*} \le X_0 < \tilde{x}_{k^*+1}$.

Now the approximate solutions $\underline{r}$ and $\underline{s}$ can be found by eliminating $\underline{q}$ from (21) and combining expressions (22), (24) and (25), to obtain, after some manipulations, a linear system of $(N + N_0 + 1)$ equations with $(N + N_0)$ unknowns as follows:

$$X\underline{w} = \underline{y}, \tag{26}$$

where

$$X = \begin{bmatrix} A^I A^{-1} D_1 - D_1^I & A^I A^{-1} D_2 - D_2^I \\ \frac{T}{N}\sum_{i=1}^{N}(A_i^{II} A^{-1} D_1 - D_{1,i}^{II}) & \frac{T}{N}\sum_{i=1}^{N}(A_i^{II} A^{-1} D_2 - D_{2,i}^{II}) \\ 0 \ldots 0 & 0 \ldots 0 \underset{\frac{1}{2}}{1} \underset{\frac{1}{2}}{1} 0 \ldots 0 \end{bmatrix}_{(N+N_0+1)\times(N+N_0)},$$

$$\underline{w} = \begin{bmatrix} \underline{r} \\ \underline{s} \end{bmatrix}_{N+N_0},$$

$$\underline{y} = \begin{bmatrix} -\underline{\chi} + A^I A^{-1}(B\underline{\mu} - C\underline{\varphi} - \underline{d}) - B^I\underline{\mu} + C^I\underline{\varphi} + \underline{d}^I \\ -\underline{\psi} + \frac{T}{N}\sum_{i=1}^{N}(A_i^{II}A^{-1}(B\underline{\mu} - C\underline{\varphi} - \underline{d}) - B_i^{II}\underline{\mu} + C_i^{II}\underline{\varphi} + \underline{d}_i^{II}) \\ S_0 \end{bmatrix}_{N+N_0+1}.$$

Since the problem is ill-posed the system of Equations (26) is ill-conditioned. In the next section, we will deal with this ill-conditioning using regularisation in order to obtain a stable solution.

4. Regularisation

In practice, the measured data is unavoidably contaminated by unplanned error. In order to model this, we add noise in the input functions $\chi(t)$ and $\psi(x)$ representing the over-determination conditions (4) and (5) as follows:

$$\underline{\chi}^p = \underline{\chi} + random('\text{Normal}', 0, \sigma_\chi, 1, N), \tag{27}$$

and

$$\underline{\psi}^p = \underline{\psi} + random('\text{Normal}', 0, \sigma_\psi, 1, N_0), \tag{28}$$

where the $random('\text{Normal}', 0, \sigma_\chi, 1, N)$ is a command in MATLAB which generates N random variables from a normal distribution with zero mean and standard deviation σ_χ, whilst the $random('\text{Normal}', 0, \sigma_\psi, 1, N_0)$ generates N_0 random variables with zero mean and standard deviation σ_ψ. Here, the standard deviations σ_χ and σ_ψ are taken as

$$\sigma_\chi = p \times \max_{t\in[0,T]} |\chi(t)|, \quad \text{and} \quad \sigma_\psi = p \times \max_{x\in[0,L]} |\psi(x)|, \tag{29}$$

where p represents the percentage of noise. Note that the measurement (6) is already contaminated by error due to the approximation made in (25).

If we consider the contamination of the right-hand side of Equation (26) as $\| \underline{y}^\epsilon - \underline{y} \| \approx \epsilon$, then the direct least-squares solution $\underline{w} = (X^{tr}X)^{-1}X^{tr}\underline{y}^\epsilon$ will be unstable. To overcome this instability, regularisation methods need to be utilised. In this study, we employ the TSVD and the Tikhonov regularisation methods.

4.1. The truncation singular value decomposition

To employ the TSVD, we first consider the decomposition of the matrix X,

$$X = U\Sigma V^{tr}, \tag{30}$$

where $U = [\underline{U}_1, \underline{U}_2, \ldots, \underline{U}_{N+N_0}]$ and $V = [\underline{V}_1, \underline{V}_2, \ldots, \underline{V}_{N+N_0}]$ are $(N + N_0 + 1) \times (N + N_0)$ matrices with columns, $\underline{U}_j$ and $\underline{V}_j$ for $j = \overline{1, (N + N_0)}$, such that $U^{tr}U = I = V^{tr}V$, and $\Sigma = \text{diag}(\sigma_1, \sigma_2, \ldots, \sigma_{N+N_0})$ is an $(N + N_0) \times (N + N_0)$ diagonal matrix containing the singular values of the matrix X, σ_j for $j = \overline{1, (N + N_0)}$, in decreasing order

$$\sigma_1 \geq \sigma_2 \geq \cdots \geq \sigma_{N+N_0} \geq 0.$$

Then the matrix system (26) can be reformed to obtain the solution as follows:

$$\underline{w} = \left(\sum_{j=1}^{N+N_0} \frac{1}{\sigma_j} \underline{V}_j \cdot \underline{U}_j^{tr} \right) \underline{y}^{\epsilon}. \tag{31}$$

In MATLAB, this decomposition is operated using the command svds$(X, N + N_0)$. For obtaining the solution of the ill-posed problem, the truncation of decomposition matrix X in (30) is needed to be considered as a regularisation method, by omitting its last $(N + N_0)$ - N_t small singular values, where N_t denotes the truncation level. This way, the regularised solution is given by

$$\underline{w}_{N_t} = \left(\sum_{j=1}^{N_t} \frac{1}{\sigma_j} \underline{V}_j \cdot \underline{U}_j^{tr} \right) \underline{y}^{\epsilon}. \tag{32}$$

In order to indicate the appropriate truncation level N_t, the L-curve criterion, the GCV method and the discrepancy principle are utilised. The L-curve method is analysed by the L-shape obtained by plotting the residual $\| X\underline{w}_{N_t} - \underline{y}^{\epsilon} \|$ versus the norm of the solution $\| \underline{w}_{N_t} \|$, for various values of N_t, (Hansen, 2001; Lesnic et al., 1998). Whilst the GCV method estimates the truncation number N_t by minimising the following GCV function, see e.g. (Bazán, 2003; Musase et al., 2004),

$$GCV(N_t) = \frac{\| X\underline{w}_{N_t} - \underline{y}^{\epsilon} \|^2}{[\text{trace}(I - XX^*)]^2} = \frac{\| XX^*\underline{y}^{\epsilon} - \underline{y}^{\epsilon} \|^2}{[\text{trace}(I - XX^*)]^2}, \tag{33}$$

where $X^* = V\Sigma_{N_t}^* U^{tr}$ is an inverse of the matrix X and $\Sigma_{N_t}^* = \text{diag}(\frac{1}{\sigma_1}, \frac{1}{\sigma_2}, \ldots, \frac{1}{\sigma_{N_t}})$. Finally, the discrepancy principle indicates the truncation number based on the knowledge of noise level

$$\epsilon = \| \underline{y}^{\epsilon} - \underline{y} \| = \sqrt{\| \underline{\chi}^p - \underline{\chi} \|^2 + \| \underline{\psi}^p - \underline{\psi} \|^2}, \tag{34}$$

by selecting the truncation number N_t such that the residual is at the same level as the noise input ϵ, i.e.

$$\| X\underline{w}_{N_t} - \underline{y}^{\epsilon} \| \approx \epsilon. \tag{35}$$

4.2. The Tikhonov regularisation

Alternatively, the Tikhonov regularisation is another way of obtaining a stable solution of the ill-conditioned system of Equations (26). This method is based on minimising the regularised linear least-squares objective function

$$\| X\underline{w} - \underline{y}^{\epsilon} \|^2 + \lambda_1 \| R_1\underline{r} \|^2 + \lambda_2 \| R_2\underline{s} \|^2 \tag{36}$$

where $R_\wp$ is a (differential) regularisation matrix corresponding to a regularisation parameter $\lambda_\wp > 0,\ \wp \in \{1,2\}$. Solving (36) one obtains the regularised solution

$$\underline{w}_{\lambda_1,\lambda_2} = (X^{tr}X + R^{tr}R)^{-1}X^{tr}\underline{y}^{\epsilon}. \tag{37}$$

where the matrix R represents a block matrix of upper-left subblock $\lambda_1 R_1$ and lower-right subblock $\lambda_2 R_2$. Here, let us call this regularisation as the block Tikhonov regularisation and choose the regularisation matrix given by either of the following expressions, (Twomey, 1963),

$$R_\wp = \begin{bmatrix} 1 & 0 & 0 & . \\ 0 & 1 & 0 & . \\ 0 & 0 & 1 & . \\ . & . & . & . \end{bmatrix}, \quad \text{the zeroth} - \text{order regularisation},$$

$$R_\wp = \begin{bmatrix} 1 & -1 & 0 & 0 & . \\ 0 & 1 & -1 & 0 & . \\ 0 & 0 & 1 & -1 & . \\ . & . & . & . & . \end{bmatrix}, \quad \text{the first} - \text{order regularisation},$$

$$R_\wp = \begin{bmatrix} 1 & -2 & 1 & 0 & 0 & . \\ 0 & 1 & -2 & 1 & 0 & . \\ 0 & 0 & 1 & -2 & 1 & . \\ . & . & . & . & . & . \end{bmatrix}, \quad \text{the second} - \text{order regularisation},$$

where $\wp \in \{1,2\}$.

Initially, we take $\lambda := \lambda_1 = \lambda_2$ and consider the L-curve criterion, the GCV method and the discrepancy principle as choices for indicating the single regularisation parameter λ. The L-curve method is based on plotting the graph of the residual $\| X\underline{w}_\lambda - \underline{y}^{\epsilon} \|$ versus the solution norm $\| \underline{w}_\lambda \|$ for a range of values of λ, (Hansen, 2001), whereas the GCV method suggests choosing the parameter λ by minimising the following GCV function, (Yan et al., 2008),

$$GCV(\lambda) = \frac{\| X\underline{w}_\lambda - \underline{y}^{\epsilon} \|^2}{[\text{trace}(I - X(X^{tr}X + \lambda R^{tr}R)^{-1}X^{tr})]^2} = \frac{\| X(X^{tr}X + \lambda R^{tr}R)^{-1}X^{tr}\underline{y}^{\epsilon} - \underline{y}^{\epsilon} \|^2}{[\text{trace}(I - X(X^{tr}X + \lambda R^{tr}R)^{-1}X^{tr})]^2}. \tag{38}$$

Note that both the L-curve and the GCV are heuristic methods because they do not require the knowledge of the level of noise ϵ. More rigorously, one can use the discrepancy principle, (Morozov, 1966), which selects λ such that

$$\| X\underline{w}_\lambda - \underline{y}^{\epsilon} \| \approx \epsilon. \tag{39}$$

If we allow for general multiple regularisation parameters λ_1 and λ_2 in (36) then, for their selection one could employ the L-surface criterion, (Belge et al., 2002), which plots the residual $\| X\underline{w}_{\lambda_1,\lambda_2} - \underline{y}^{\epsilon} \|$ versus $\| R_1\underline{r} \|$ and $\| R_2\underline{s} \|$ for various values of λ_1 and λ_2.

5. Numerical examples and discussion

To test the accuracy of the approximate solutions, let us introduce the root mean square error (RMSE) defined as

$$\mathrm{RMSE}(r(t)) = \sqrt{\frac{T}{N}\sum_{i=1}^{N}(r_{exact}(\tilde{t}_i) - r_{numerical}(\tilde{t}_i))^2}, \tag{40}$$

and

$$\mathrm{RMSE}(s(x)) = \sqrt{\frac{L}{N_0}\sum_{k=1}^{N_0}(s_{exact}(\tilde{x}_k) - s_{numerical}(\tilde{x}_k))^2}. \tag{41}$$

5.1. *Example 1*

In the first example, we consider a smooth benchmark test with $T = L = 1$, $X_0 = \frac{1}{2}$ and the input data

$$\begin{cases} \varphi(x) = u(x,0) = x^2, \quad \mu_0(t) = u(0,t) = 0, \quad \mu_1(t) = u(1,t) = e^t, \\ \chi(t) = u(\frac{1}{2},t) = \frac{e^t}{4}, \quad \psi(x) = \int_0^1 u(x,t)\,dt = x^2(e-1), \quad S_0 = s(\frac{1}{2}) = 1, \\ f(x,t) = e^x, \quad g(x,t) = t+1, \quad h(x,t) = (x^2-2)e^t - t^2e^x - (t+1)\sin(\pi x). \end{cases} \tag{42}$$

One can check that the conditions of Theorem 1 are satisfied hence the inverse source problem (1)–(6) with the data (42) has a unique solution. It can easily be verified through direct substitution that this solution is given by

$$u(x,t) = x^2e^t, \quad r(t) = t^2, \quad s(x) = \sin(\pi x). \tag{43}$$

As mentioned in Section 2, the inverse heat source problem (1)–(6) is ill-posed since small errors in the measured data (4)–(6) cause large errors in the solution. In order to quantify the degree of ill-conditioning, we calculate the condition number of the matrix X. The condition numbers for $N = N_0 \in \{20, 40, 80\}$ and $X_0 \in \{\frac{1}{4}, \frac{1}{2}, \frac{3}{4}\}$ are shown in Table 1. In addition, the normalised singular values of the matrix X are displayed in Figure 1, and the rapidly decreasing values indicate that the system of Equations (26) is ill-conditioned. Looking at the columns of Table 1 it can be seen that the condition number only slightly decreases as X_0 increase, hence we do not expect the numerical results to be significantly influenced by the choice of X_0 within some interval $[\frac{1}{4}, \frac{3}{4}]$ away

Table 1. The condition numbers of the matrix X in Equation (26) for various $N = N_0 \in \{20, 40, 80\}$ and $X_0 \in \{\frac{1}{4}, \frac{1}{2}, \frac{3}{4}\}$.

$N = N_0$	20	40	80
$X_0 = 1/4$	1.94E+3	9.07E+3	5.04E+4
$X_0 = 1/2$	1.97E+3	7.51E+3	4.06E+4
$X_0 = 3/4$	1.93E+3	6.50E+3	3.33E+4

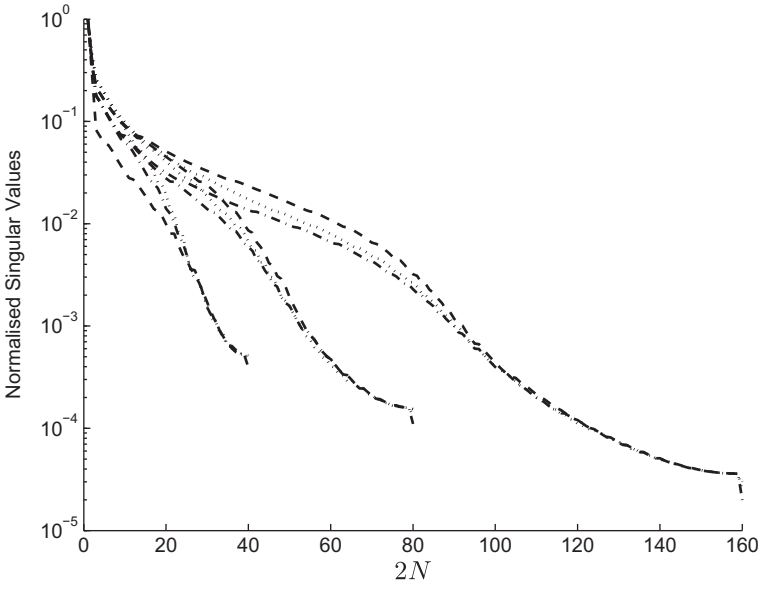

Figure 1. The normalised singular values of matrix X for $N = N_0 \in \{20, 40, 80\}$ and $X_0 \in \{\frac{1}{4}(- \cdot -), \frac{1}{2}(\cdots), \frac{3}{4}(- - -)\}$, for Example 1.

from the end points $x = 0$ and $x = L = 1$. Of course, as X_0 gets closer to the boundary point $x = 0$ or $x = L$ then the specification of the interval temperature measurement (4) resembles a heat flux prescription, namely

$$u_x(0,t) = \lim_{X_0 \searrow 0} \frac{u(X_0,t) - u(0,t)}{X_0}, \quad \text{or} \quad u_x(L,t) = \lim_{X_0 \nearrow L} \frac{u(X_0,t) - u(L,t)}{X_0 - L}.$$

However, this newly generated inverse problem in which Cauchy data are specified at $x = 0$ or $x = L$ is not addressed herein and it is deferred to a future work.

In what follows, the numerical results are illustrated for a fixed discretisation $N = N_0 = 40$ and $X_0 = \frac{1}{2}$.

5.1.1. *Exact data*

We consider first the case of exact data, i.e. $p = 0$ in (29). We directly solve the linear system of Equations (26) with the untruncated SVD method, and display the numerical solutions for $r(t)$, $s(x)$, $u_x(0, t)$ and $u_x(1, t)$ in Figures 2(a)–2(d), respectively.

From these figures, it can be seen that the solutions for $r(t)$ and $s(x)$ are inaccurate, but the fluxes $u_x(0, t)$ and $u_x(1, t)$ are stable and accurate with small RMSEs of 9.32E-3 and 4.58E-2, respectively, see Table 2. This is somewhat to be expected since the inverse problem is ill-posed. Hence, regularisation is required to overcome this instability.

For this, we utilise the TSVD and the Tikhonov regularisation of orders zero, one and two. The selection method of the regularisation parameters is first considered. The L-curves of the TSVD and the Tikhonov regularisations are presented in Figures 3(a) and 4(a), respectively. It can be seen that there is no L-shape obtained for either the TSVD, the zeroth-, or the first-order Tikhonov regularisations, whereas the

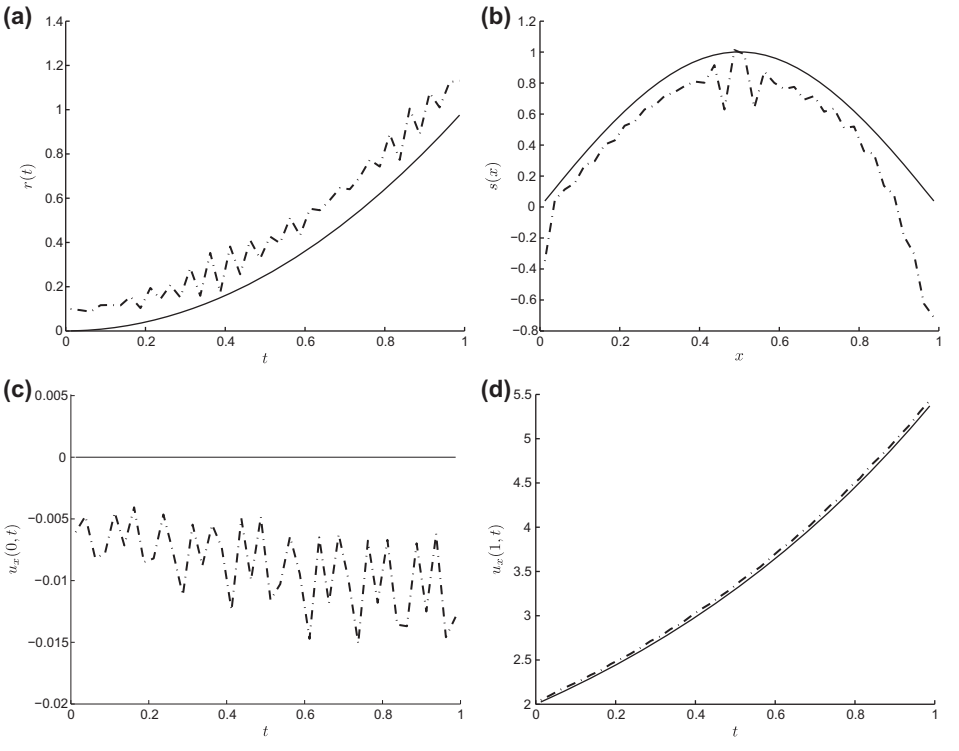

Figure 2. The analytical (—) and numerical results (– · –) of (a) $r(t)$, (b) $s(x)$, (c) $u_x(0, t)$, and (d) $u_x(1, t)$ obtained using the SVD for exact data, for Example 1.

second-order Tikhonov regularisation shows more clearly an L-corner at λ = 1E-1. Alternatively, the GCV method is utilised as another choice for the regularisation parameter, as shown in Figure 3(b). The minimum of the GCV function suggests $N_t = 56$ to be the truncation number for the TSVD, whilst for the Tikhonov regularisation which is displayed in Figure 4(b), the minima indicate the parameters λ = 1.0E-7, 1.2E-7 and 4.5E-8 for orders zero, one and two, respectively. Note that for the exact data, $\epsilon \approx 0$ and the discrepancy principle cannot be employed.

With the GCV selection for the regularisation parameters determined from Figures 3(b) and 4(b), the TSVD and the Tikhonov regularisation results are shown in Figure 5. Compared to Figure 2, one can see that the instability of the numerical solutions is not alleviated. We then employ another choice of the regularisation parameter based on the L-curve method. This suggests λ = 1E-1 for the second-order Tikhonov regularisation displayed in Figure 4(b). Then with this choice for λ we obtain the stable and accurate numerical results shown in Figure 6 and Table 2.

5.1.2. *Noisy data*

Next, the case of noise contamination with percentage p = 1% is considered by adding random noise into the input functions $\chi(t)$ and $\psi(x)$ in (42), as in (27) and (28), respectively. It is of crucial importance to utilise the regularisation in this case, and selecting the regularisation parameters is the first step of the regularisation process.

Table 2. The RMSE for $r(t)$, $s(x)$, $u_x(0, t)$, and $u_x(1, t)$ obtained using the SVD, the TSVD and the Tikhonov regularisation of orders zero, one, and two, for $p \in \{0, 1\}\%$, for Example 1.

Method	p	Parameter	RMSE			
			$r(t)$	$s(x)$	$u_x(0, t)$	$u_x(1, t)$
SVD	0	–	1.47E–1	2.55E–1	9.32E–3	4.58E–2
TSVD	0	$N_t = 56$	1.17E–1	2.03E–1	2.94E–3	3.57E–2
Zeroth	0	$\lambda = 1.0$E–7	1.20E–1	2.02E–1	3.53E–3	3.65E–2
First	0	$\lambda = 1.2$E–7	7.62E–2	1.70E–1	3.68E–3	4.35E–2
Second	0	$\lambda = 4.5$E–8	7.96E–2	1.85E–1	6.48E–3	4.70E–2
Second	0	$\lambda = 1.0$E–1	8.70E–3	2.81E–2	1.27E–2	3.09E–3
SVD	1%	–	1.62E+1	1.01E+2	2.84	2.48E–1
TSVD	1%	$N_t = 14$	2.04E–1	1.77E–1	2.29E–2	5.83E–2
Zeroth	1%	$\lambda = 1.3$E–3	1.87E–1	1.83E–1	2.32E–2	4.87E–2
First	1%	$\lambda = 2.8$E–2	1.28E–1	3.50E–1	1.05E–1	7.91E–2
Second	1%	$\lambda = 1.5$	9.72E–2	2.65E–1	8.05E–2	5.58E–2
Second	1%	$\lambda = 10$	1.61E–1	4.23E–1	1.20E–1	9.36E–2
Second	1%	$\lambda_1 = 10$, $\lambda_2 = 1$	7.93E–2	2.18E–1	6.81E–2	4.40E–2
Second	1%	$\lambda_1 = 8$,$\lambda_2 = 5.2$E–2	1.92E–3	5.34E–2	1.00E–2	6.39E–3

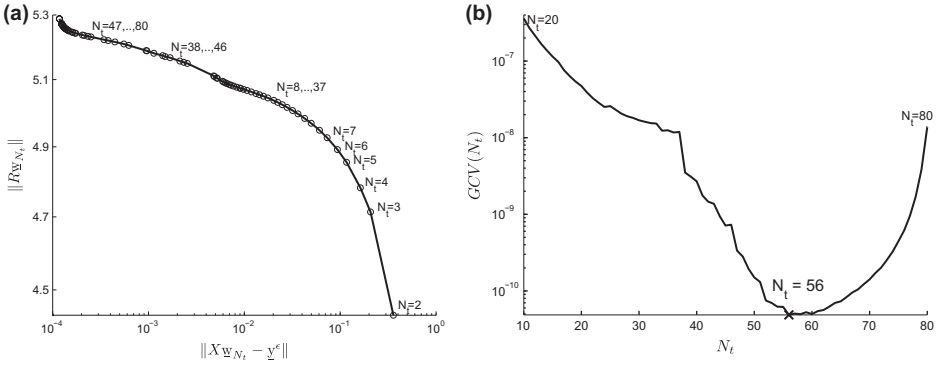

Figure 3. (a) The L-curve and (b) the GCV function obtained by the TSVD for exact data, for Example 1.

Here, the L-curve method and the discrepancy principle are employed as criteria for choosing the regularisation parameters. These are displayed in Figures 7 and 8 using the TSVD and the Tikhonov regularisation, respectively. The suggested parameters are given in Table 2. Figure 9 presents all results obtained using the TSVD and the Tikhonov regularisation of orders zero, one and two with the regularisation parameters suggested by the discrepancy principle, see Table 2. Looking more closely at Figure 9(a), it can be seen that the approximate solutions for $r(t)$ obtained by the first- and the second-order Tikhonov regularisation are reasonably stable, whereas the numerical solution for $s(x)$, as shown in Figure 9(b) is rather inaccurate.

We consider the second-order Tikhonov regularisation with the regularisation parameter suggested by the L-curve method $\lambda = 10$ and obtain the results shown in Figure 11. After analysing this numerical solution, it can be clearly observed that we cannot obtain accurate solutions for both r and s using $\lambda_1 = \lambda_2$. Therefore, the case

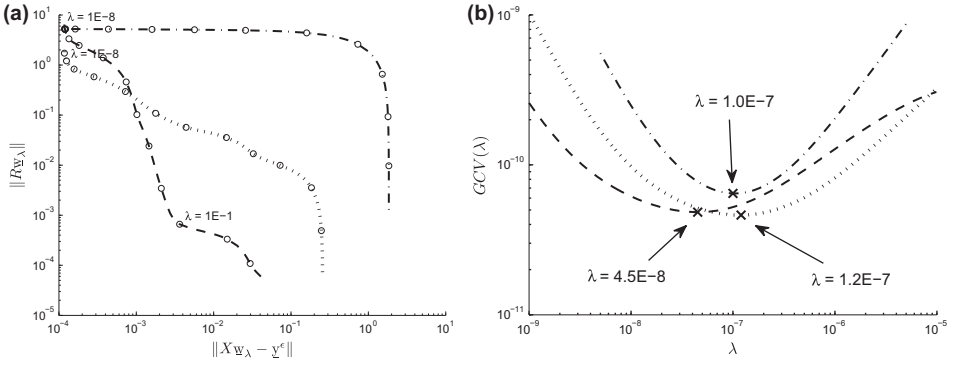

Figure 4. (a) The *L*-curve, and (b) the GCV function, obtained by the Tikhonov regularisation of order zero (– · –), one (···) and two (– – –) for exact data, with $\lambda = \lambda_1 = \lambda_2$, for Example 1.

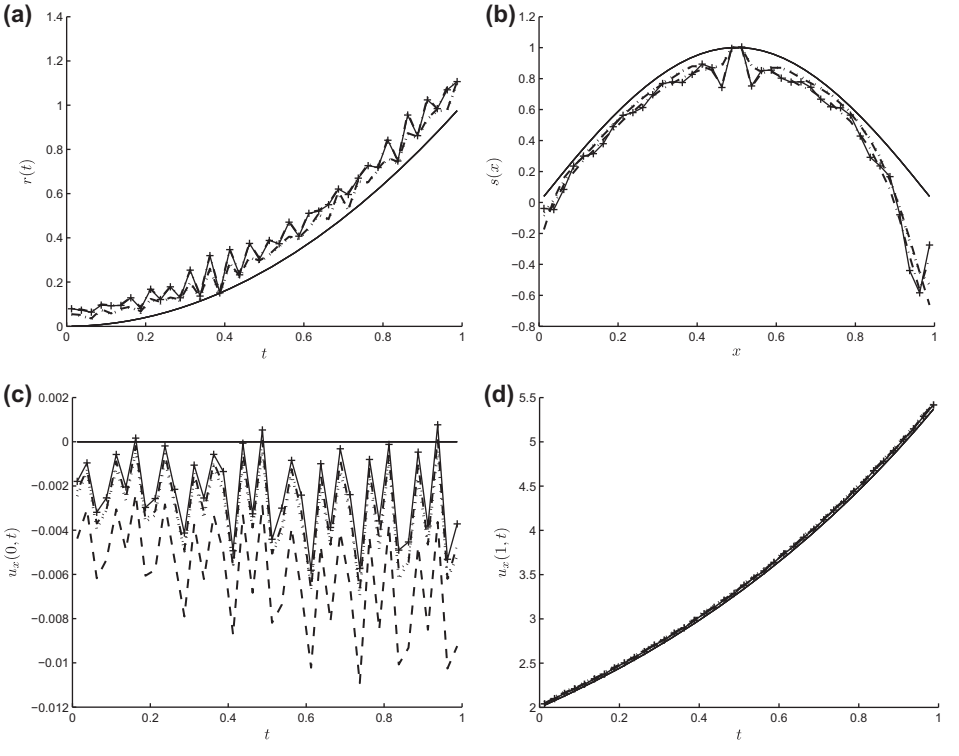

Figure 5. The analytical (—) and numerical results of (a) $r(t)$, (b) $s(x)$, (c) $u_x(0, t)$, and (d) $u_x(1, t)$ obtained using the TSVD (– + –), and the Tikhonov regularisation of orders zero (– · –), one (···), and two (– – –) with regularisation parameters suggested by the GCV function of Figure 3(b) and 4(b) for exact data, for Example 1.

$\lambda_1 \neq \lambda_2$ is considered and the *L*-surfaces are shown in Figure 10. On the plane of logarithm of residual norm, $\log \| Xw_\lambda - y^\varepsilon \|$, versus logarithm of the second-order derivative of r, $\log \| R_1 r_{\lambda_1} \|$, there is an *L*-shaped corner at λ_1 = 1E + 1, while λ_2 = 1

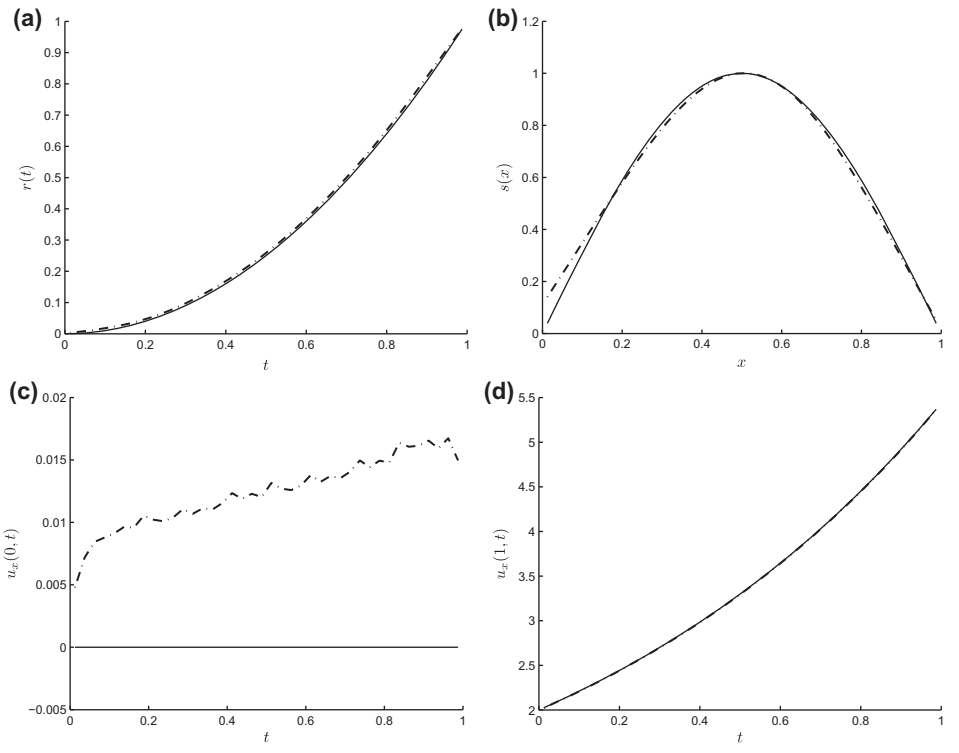

Figure 6. The analytical (—) and numerical results (– · –) of (a) $r(t)$, (b) $s(x)$, (c) $u_x(0, t)$, and (d) $u_x(1, t)$ obtained using the second-order Tikhonov regularisation with the regularisation parameter $\lambda_1 = \lambda_2 = \lambda = 1E - 1$ suggested by the L-curve of Figure 4(a) for exact data, for Example 1.

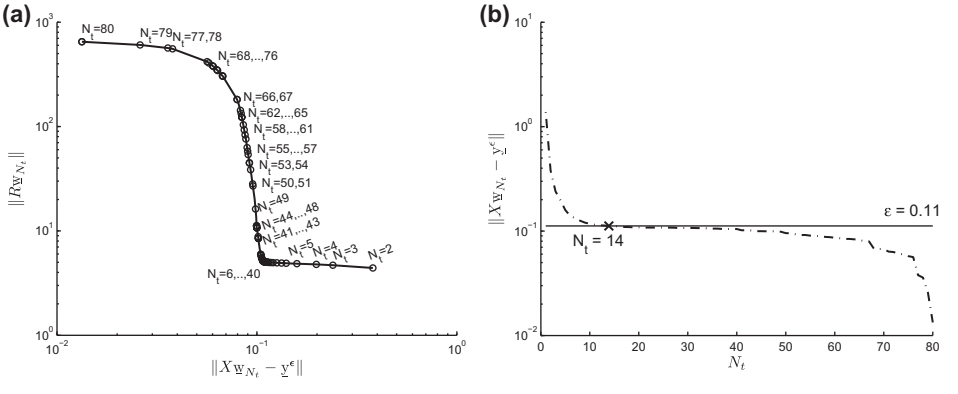

Figure 7. (a) The L-curve and (b) the discrepancy principle obtained using the TSVD for noisy input p = 1%, for Example 1.

is based around the area of the L-corner on the plane of $\log \| Xw_\lambda - y^\epsilon \|$ versus $\log \| R_2 r_{\lambda_2} \|$. However, the numerical solution for $s(x)$ obtained using the parameters $\lambda_1 = 10$, $\lambda_2 = 1$ suggested by the L-surface method, is still inaccurate. We finally use

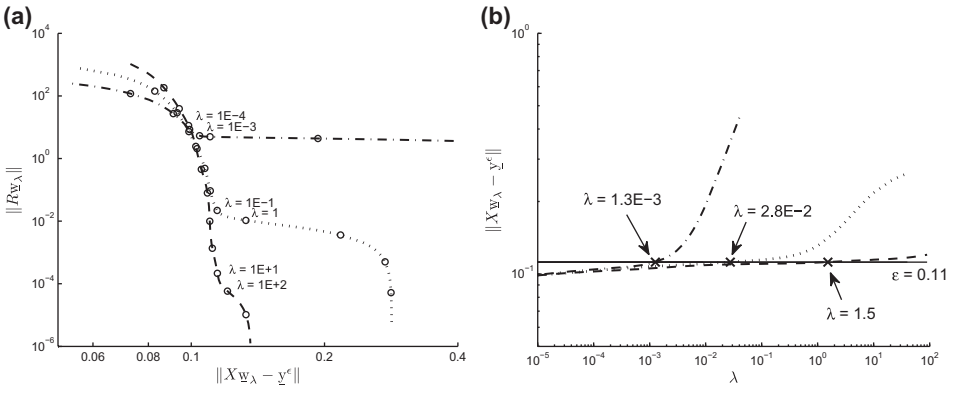

Figure 8. (a) The *L*-curve and (b) the discrepancy principle obtained using the Tikhonov regularisation of order zero (– · –), one (···), and two (– – –) for noisy input p = 1%, with $\lambda = \lambda_1 = \lambda_2$, for Example 1.

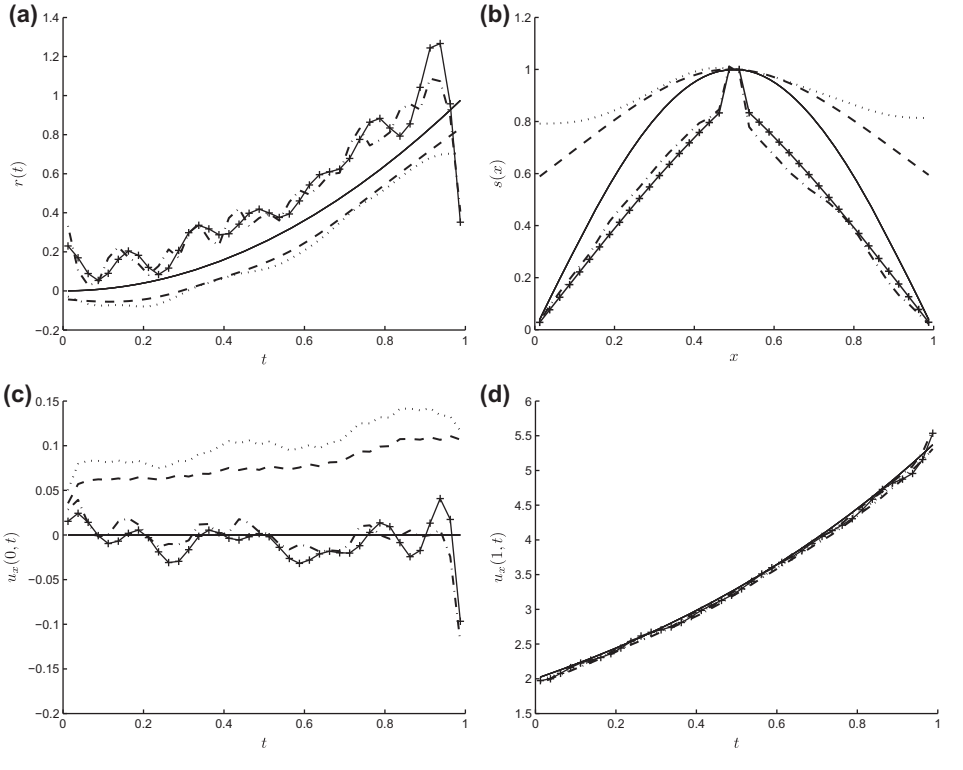

Figure 9. The analytical (—) and numerical results of (a) $r(t)$, (b) $s(x)$, (c) $u_x(0, t)$, and (d) $u_x(1, t)$ obtained using the TSVD (– + –) with N_t = 14, and the Tikhonov regularisation of orders zero (– · –), one (···), and two (– – –) with regularisation parameters suggested by the discrepancy principle of Figure 8(b) for noisy input p = 1%, for Example 1.

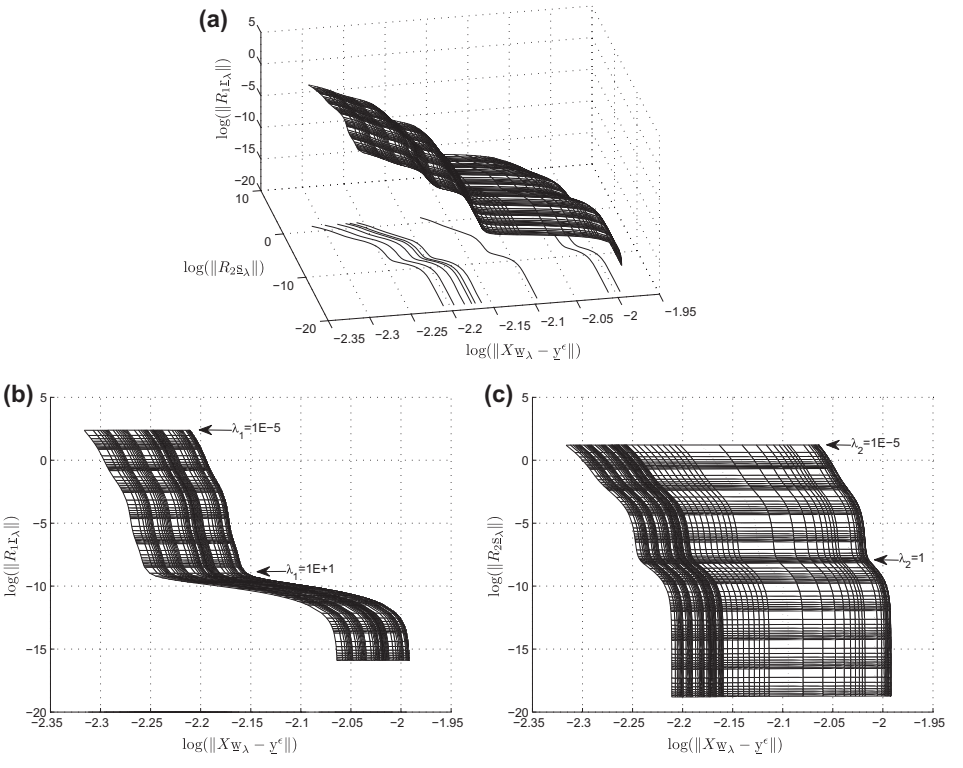

Figure 10. The L-surface on (a) a three-dimensional plot, (b) plane of $\log \| X\underline{w}_\lambda - \underline{y}^\epsilon \|$ versus $\log \| R_1\underline{r}_\lambda \|$, and (c) plane of $\log \| X\underline{w}_\lambda - \underline{y}^\epsilon \|$ versus $\log \| R_2\underline{s}_\lambda \|$, obtained using the second-order Tikhonov regularisation for noisy input $p = 1\%$, for Example 1.

the trial and error process to seek out the appropriated regularisation parameters, and found that regularisation parameters $\lambda_1 = 8$ and $\lambda_2 = 5.2\text{E-}2$ can yield an accurate and stable numerical solution, see Figure 11. Nevertheless, more research has to be undertaken in the future for the selection of appropriate multiple regularisation parameters, (Chen, Lu, Xu, & Yang, 2008).

The RMSE of all results which we have mentioned so far are detailed in Table 2.

5.2. *Example 2*

Let $T = L = 1$, $X_0 = \frac{1}{2}$ and the input data

$$\begin{cases} \varphi(x) = \mu_0(t) = \mu_1(t) = 0, \quad S_0 = s(\frac{1}{2}) = \frac{1}{4}, \quad \chi(t) = u(\frac{1}{2}, t) = t^2 \sin(\frac{1}{4}), \\ \psi(x) = \int_0^1 u(x,t)\, dt = \frac{\sin(x-x^2)}{3}, \quad f(x,t) = x, \quad g(x,t) = e^t, \\ h(x,t) = (2t + t^2(1-2x)^2)\sin(x-x^2) + 2t^2\cos(x-x^2) - x|t - \frac{1}{2}| - e^t|x - \frac{3}{4}|. \end{cases} \tag{44}$$

Note that the input data (44) satisfy the conditions of Theorem 1 to ensure the existence and uniqueness of solution of the inverse problem (1)–(6). In fact, the exact solution is given by

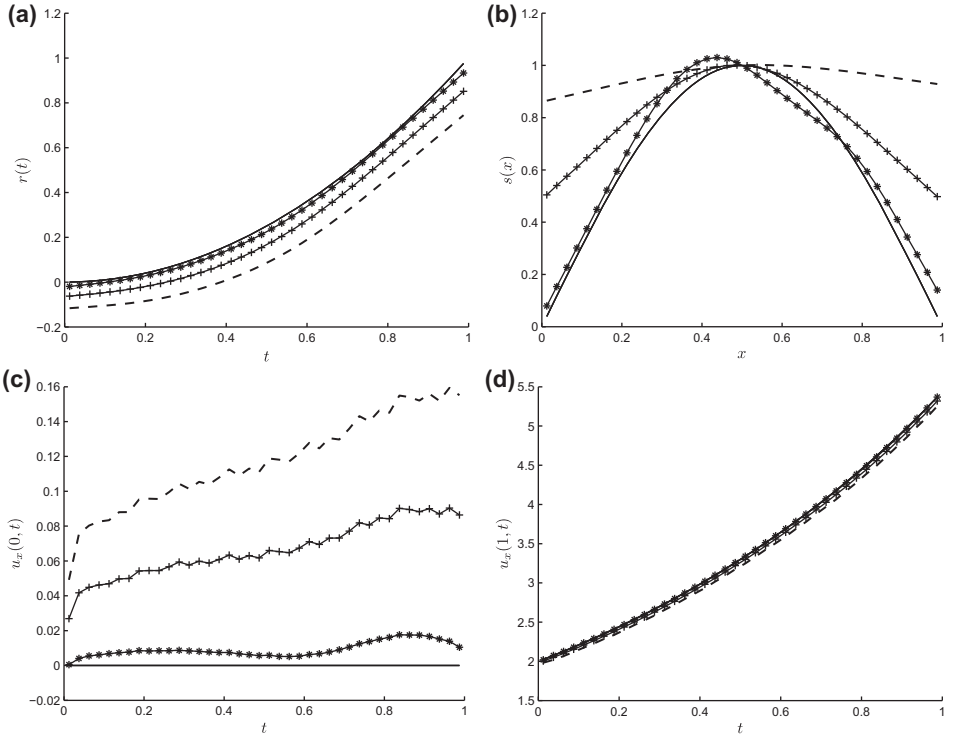

Figure 11. The analytical (—) and numerical results of (a) $r(t)$, (b) $s(x)$, (c) $u_x(0, t)$, and (d) $u_x(1, t)$ obtained using the second-order Tikhonov regularisation with regularisation parameters suggested by the L-curve criterion $\lambda = \lambda_1 = \lambda_2 = 10$ (– – –), the L-surface method (λ_1, λ_2)= (10,1) (– + –), and the trial and error (λ_1, λ_2)=(8,5.2E-2) (– ∗ –), for noisy input p = 1%, for Example 1.

$$u(x,t) = t^2 \sin(x - x^2), \quad r(t) = |t - \frac{1}{2}|, \quad s(x) = |x - \frac{3}{4}|.$$

This is a more severe test example than Example 1 since the source components $r(t)$ and $s(x)$ are not smooth functions.

We have calculated the condition numbers of the matrix X and obtained the condition numbers 3.46E+3, 1.54E+4 and 8.69E+4 for $N = N_0 =$ 20, 40 and 80, respectively. Moreover, the corresponding normalised singular values are shown in Figure 12.

In Example 2, the condition numbers of the matrix X are not much different from the condition numbers for Example 1. Then we expect to solve this inverse problem by using the TSVD, or the Tikhonov regularisation as means to reduce the instability of the solution. We fix $N = N_0 = 40$ and $X_0 = \frac{1}{2}$.

5.2.1. *Exact data*

First, we have tried the TSVD and the Tikhonov regularisation of orders zero, one and two with the regularisation parameter given by the GCV function. This yields N_t = 65, λ = 2.9E-8, 3.2E-8 and 8.3E-9, respectively. But we have found that the numerical solutions for $r(t)$ and $s(x)$ are not so accurate. We then considered the L-curve method for choosing the regularisation parameter. Figures 13(a) and 13(b) display the L-curves for the TSVD and the Tikhonov regularisation, respectively. The same as the L-curve

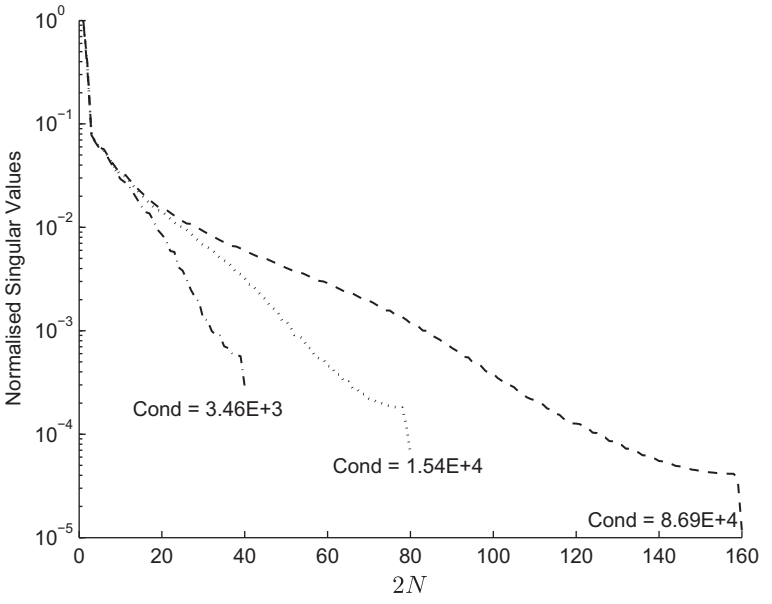

Figure 12. The normalised singular values of matrix X for $N = N_0 = 20$ (– · –), $N = N_0 = 40$ (···), and $N = N_0 = 80$ (– – –), for Example 2.

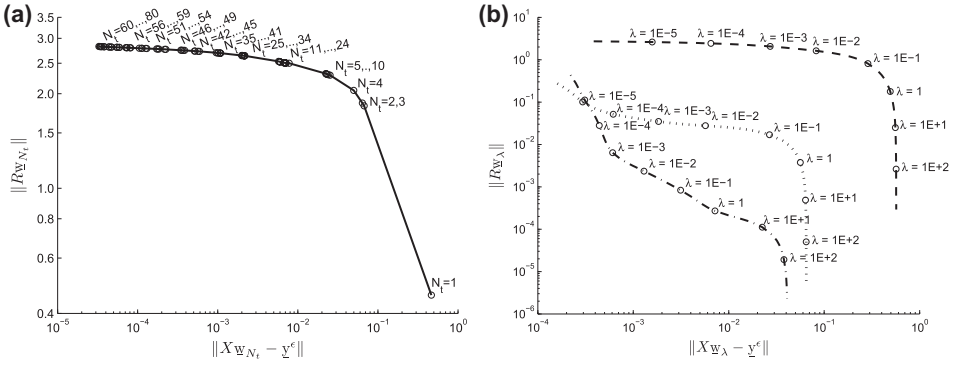

Figure 13. The L-curve obtained using (a) the TSVD and (b) the Tikhonov regularisation of orders zero (– · –), one (···) and two (– – –) with $\lambda = \lambda_1 = \lambda_2$, for exact data, for Example 2.

in Example 1, an L-shape is obtained only when using the second-order Tikhonov regularisation. This suggests an L-corner around λ = 1E-4 to 1E-3. In particular, for λ = 1E-4, we obtain the stable solutions presented in Figure 14 and Table 3. The untruncated SVD, i.e. N_t = 80, whose numerical results are also included is not so accurate and stable in retrieving the functions $r(t)$ and $s(x)$.

5.2.2. *Noisy data*

When noise is present in the measured data $\chi(t)$ and $\psi(x)$, the regularisation with an appropriate parameter has to be carefully considered. Here, we have tried solving the

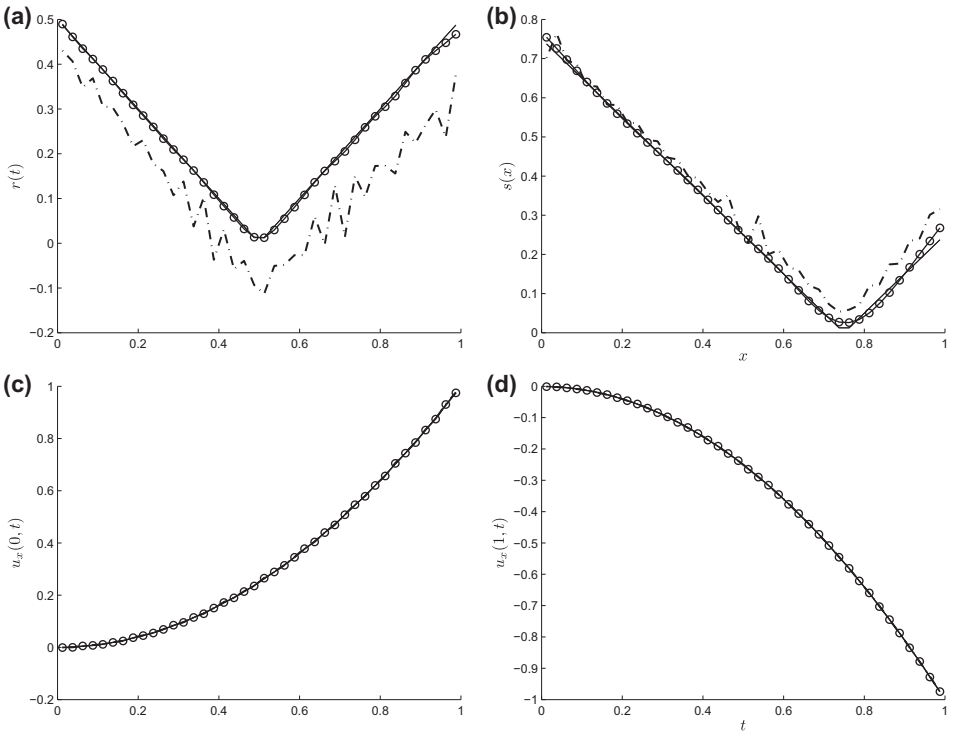

Figure 14. The analytical (—) and numerical results of (a) $r(t)$, (b) $s(x)$, (c) $u_x(0, t)$, and (d) $u_x(1, t)$ obtained using the SVD (– · –) and the second-order Tikhonov regularisation (–o–) with the regularisation parameter $\lambda_1 = \lambda_2 = \lambda$ = 1E-4 suggested by the L-curve of Figure 13(b) for exact data, for Example 2.

Table 3. The RMSE for $r(t)$, $s(x)$, $u_x(0, t)$, and $u_x(1, t)$ obtained using the SVD, the TSVD, and the Tikhonov regularisation of orders zero, and two, for $p \in \{0, 1\}$%, for Example 2.

			RMSE			
Method	p	Parameter	$r(t)$	$s(x)$	$u_x(0, t)$	$u_x(1, t)$
SVD	0	–	1.15E–1	4.12E–2	2.05E–3	6.95E–4
TSVD	0	$N_t = 65$	1.17E–1	7.92E–2	1.15E–1	4.12E–2
Zeroth	0	$\lambda = 2.9$E–8	1.67E–1	6.63E–2	5.21E–3	2.19E–3
First	0	$\lambda = 3.2$E–8	8.94E–2	2.99E–2	2.12E–3	6.01E–4
Second	0	$\lambda = 8.3$E–9	9.20E–2	3.13E–2	2.10E–3	7.61E–4
Second	0	$\lambda = 1.0$E–4	5.88E–3	8.94E–3	2.39E–3	1.04E–3
SVD	1%	-	5.31E+1	8.91E+1	2.88	2.42E–1
TSVD	1%	$N_t = 10$	2.16E–1	2.37E–1	1.15E–1	9.05E–2
Zeroth	1%	$\lambda = 7.3$E–4	1.20E–1	2.12E–1	1.15E–1	4.72E–2
First	1%	$\lambda = 3.2$E–2	1.66E–1	6.77E–2	2.21E–2	2.51E–2
Second	1%	$\lambda = 2.3$	5.78E–2	7.90E–2	9.98E–3	4.95E–2
Second	1%	$\lambda = 1$	9.24E–2	6.63E–2	1.55E–2	4.04E–2
Second	1%	$\lambda_1 = 1, \lambda_2 = 10$	3.96E–2	1.13E–1	4.67E–3	6.40E–2
Second	1%	$\lambda_1 = 2.2, \lambda_2 = 5.9$	2.37E–2	1.01E–1	3.42E–3	5.98E–2

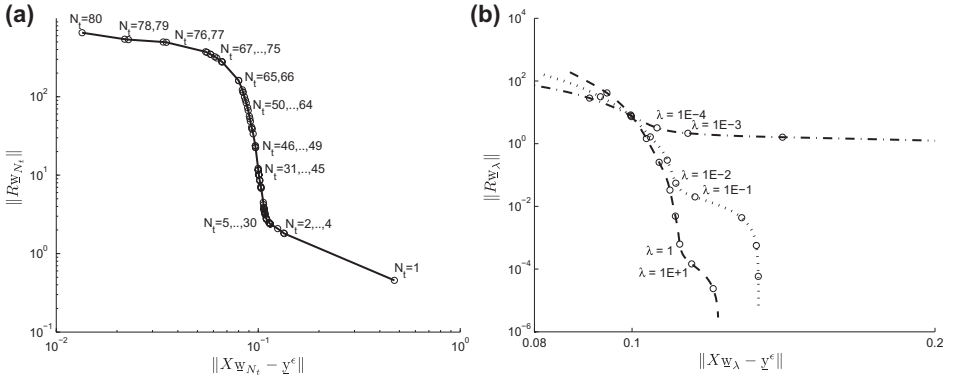

Figure 15. The *L*-curve obtained using (a) the TSVD and (b) the Tikhonov regularisation of orders zero (– · –), one (···), and two (– – –) with $\lambda = \lambda_1 = \lambda_2$, for noisy input p = 1%, for Example 2.

perturbed problem with p = 1% noisy input by using the TSVD and the Tikhonov regularisation of orders zero, one, and two with the regularisation parameter given by the discrepancy principle. This yields N_t = 10, λ = 7.3E-4, 3.2E-2 and 2.3, respectively. Although the discrepancy principle is a rigorous method which uses the knowledge of

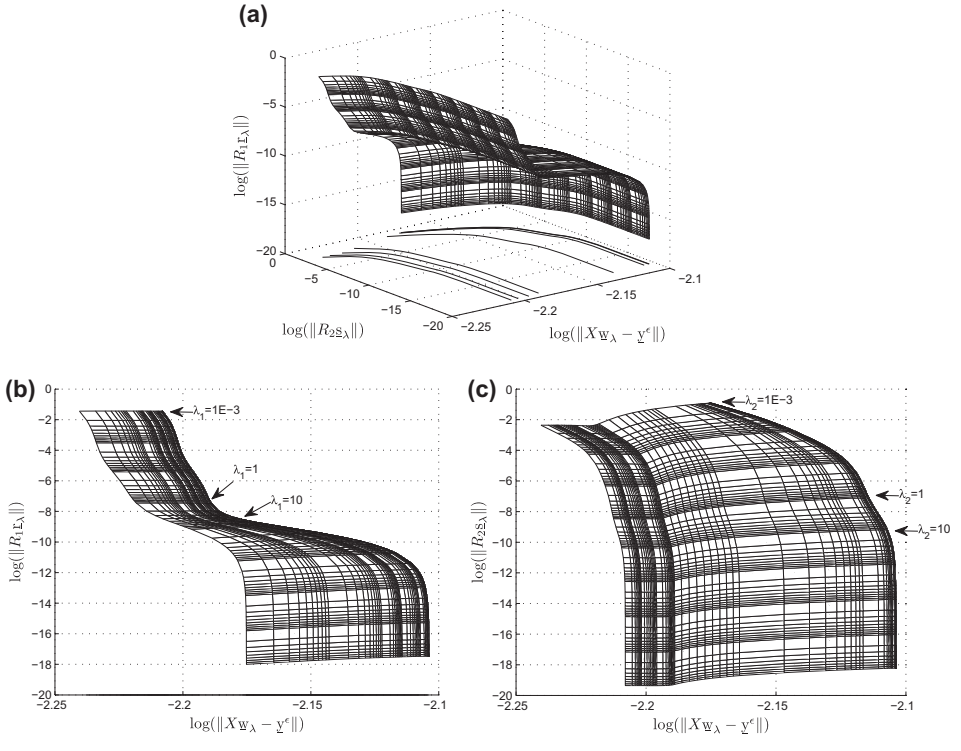

Figure 16. The *L*-surface on (a) a three-dimensional plot, (b) plane of $\log \| X\underline{w}_\lambda - \underline{y}^\epsilon \|$ versus $\log \| R_1\underline{r}_\lambda \|$, and (c) plane of $\log \| X\underline{w}_\lambda - \underline{y}^\epsilon \|$ versus $\log \| R_2\underline{s}_\lambda \|$, obtained using the second-order Tikhonov regularisation for noisy input p = 1%, for Example 2.

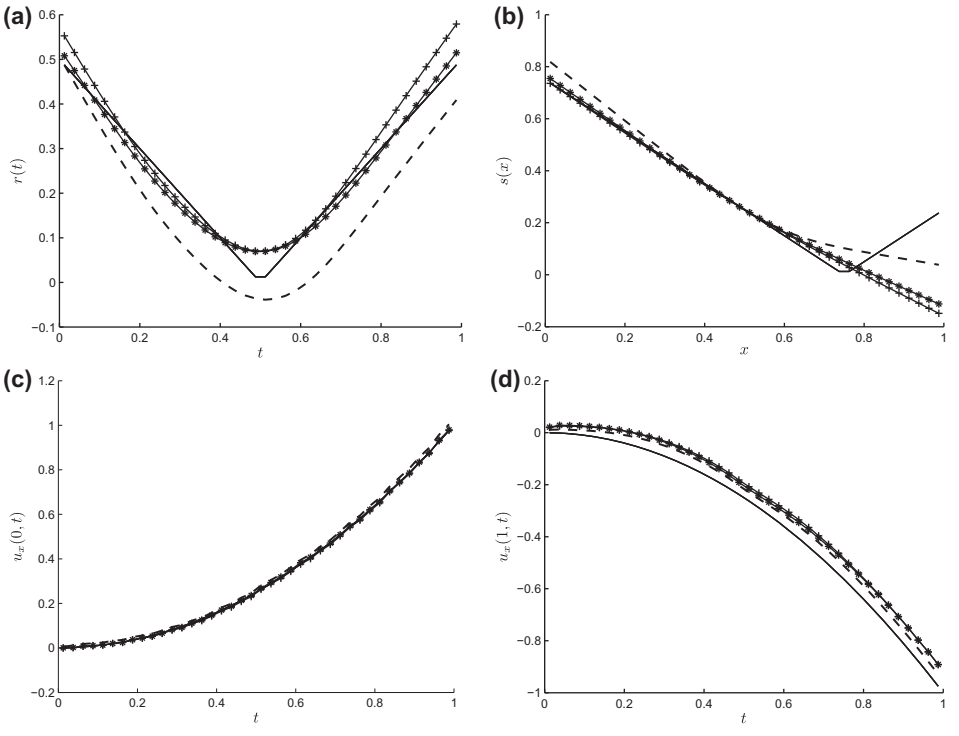

Figure 17 The analytical (—) and numerical results of (a) $r(t)$, (b) $s(x)$, (c) $u_x(0, t)$, and (d) $u_x(1, t)$ obtained using the second-order Tikhonov regularisation with regularisation parameters suggested by the L-curve criterion $\lambda = \lambda_1 = \lambda_2 = 1$ (– – –), the L-surface method (λ_1, λ_2)=(1,10) (– + –), and the trial and error (λ_1, λ_2)=(2.2,5.9) (– ∗ –), for noisy input p = 1%, for Example 2.

noise, the RMSE errors displayed in Table 3 are quite large. Alternatively, we consider the L-curve method for the choice of regularisation parameter displayed in Figure 15. This suggests the appropriate parameters as $N_t \in \{5, \ldots, 30\}$, λ = 1E-4, 1E-2, and 1 for the TSVD and the Tikhonov regularisation of orders zero, one and two, respectively. We then solved the inverse problem with these parameters and found that the numerical results obtained using the TSVD, zero- and first-order Tikhonov regularisation are not so accurate. Whereas the second-order Tikhonov regularisation yields an accurate solution, as shown in Figure 17 with dashed line. Hence, as in Example 1, the case of $\lambda_1 \neq \lambda_2$ needs to be considered by using the L-surface method for choosing the appropriate regularisation parameters. Figures 16 displays the L-surface which selects λ_1 = 10 and λ_2 = 1 and the results obtained using the second-order Tikhonov regularisation with these parameters are shown in Figure 17. Furthermore, the regularisation parameters selected by the trial and error have also been considered and these results have also been included in Figure 17. The accurate and stable retrieval of $r(t)$ is possible, but for $s(x)$ this is less accurate.

6 Conclusions

This paper has presented a numerical approach to the simultaneous numerical determination of the space- and the time-dependent coefficient source functions of an inverse

heat conduction problem with Dirichlet boundary conditions together with specified interior temperature measurement and time-integral condition, as the over-determination conditions.

The numerical discretisation was based on the BEM together with either the TSVD, or the Tikhonov regularisation. Additionally, various methods for choosing the regularisation parameters have been utilised. The numerical results presented show that accurate and stable numerical solutions can be achieved provided that the regularisation parameters are appropriately selected. The two-parameter selection has proved to be difficult, as some of our numerical results obtained using several criteria, e.g. discrepancy principle, GCV, *L*-curve, *L*-surface, have shown. Nevertheless, more research has to be undertaken in the future for the selection of multiple regularisation parameters, (Chen et al., 2008). At present, we are investigating an iterative process of regularisation, (Hào, Thanh, Lesnic, & Kerimov, 2013), whose stopping criterion based on the single choice of the iteration number does not involve the choice of two Tikhonov regularisation parameters.

Future work will also consist of constructing multiplicative space- and time-dependent heat sources, (Savateev, 1995).

Acknowledgements

A. Hazanee would like to acknowledge the financial support received from the Ministry of Science and Technology of Thailand, and Prince of Songkla University Thailand, for pursuing her PhD at the University of Leeds. Fruitful discussion with Professor M.Ivanchov is also acknowledged. The comments and suggestions made by the referees are gratefully acknowledged.

References

Ahmadabadi, M. N., Arab, M., & Maalek-Ghaini, F. M. (2009). The method of fundamental solutions for the inverse space-dependent heat source problem. *Engineering Analysis with Boundary Elements, 33*, 1231–1235.

Bazán, F. S. V. (2003). CGLS-GCV: A hybrid algorithm for low-rank-deficient problems. *Applied Numerical Mathematics, 47*, 91–108.

Belge, M., Kilmer, M., & Miller, E. L. (2002). Efficient determination of multiple regularisation parameters in a generalised *L*-curve framework. *Inverse Problems, 18*, 1161–1183.

Chen, Z., Lu, Y., Xu, Y., & Yang, H. (2008). Multi-parameter Tikhonov regularisation for linear ill-posed operator equations. *Journal of Computational Mathematics, 26*, 37–55.

Farcas, A., & Lesnic, D. (2006). The boundary element method for the determination of a heat source dependent on one variable. *Journal of Engineering Mathematics, 54*, 375–388.

Hansen, P. C. (2001). The *L*-curve and its use in the numerical treatment of inverse problems. In P. Johnston (Ed.), *Computational Inverse Problems in Electrocardiology* (pp. 119–142). Southampton: WIT Press.

Hào, D. N., Thanh, P. X., Lesnic, D., & Ivanchov, M. (2013). Determination of a source in the heat equation from integral observations. *Submitted to Journal of Computational and Applied Mathematics*.

Hazanee, A., Ismailov, M. I., Lesnic, D., & Kerimov, N. B. (2013). An inverse time-dependent source problem for the heat equation. *Applied Numerical Mathematics, 69*, 13–33.

Hazanee, A., & Lesnic, D. (2013). Determination of a time-dependent heat source from nonlocal boundary conditions. *Engineering Analysis with Boundary Elements, 37*, 936–956.

Ismailov, M. I., Kanca, F., & Lesnic, D. (2011). Determination of a time-dependent heat source under nonlocal boundary and integral overdetermination conditions. *Applied Mathematics and Computation, 218*, 4138–4146.

Ivanchov, M. I. (2001). Inverse problem for a multidimensional heat equation with an unknown source function. *Matematychni Studii, 16*, 93–98.

Ladyženskaja, O. A., Solonnikov, V. A., & Ural'ceva, N. N. (1968). *Linear and Quasi-linear Equations of Parabolic Type*. Providence, RI: American Mathematical Society.

Lesnic, D., Elliott, L., & Ingham, D. B. (1998). The boundary element solution of the Laplace and biharmonic equations subjected to noisy boundary data. *International Journal for Numerical Methods in Engineering, 43*, 479–492.

Morozov, A. (1966). On the solution of functional equations by the method of regularisation. *Soviet Mathematics Doklady, 7*, 414–417.

Musase, K., Yamazaki, Y., & Miyazaki, S. (2004). Deconvolution analysis of dynamic contrast-enhanced data based on singular value decomposition optimised by generalised cross validation. *Magnetic Resonance in Medical Sciences, 3*, 165–175.

Prilepko, A. I., & Solov'ev, V. V. (1988). Solvability theorems and Rothe's method for inverse problems for a parabolic equation. I. *Differential Equations, 23*, 1230–1237.

Prilepko, A. I., & Tkachenko, D. S. (2003). Inverse problem for a parabolic equation with integral overdetermination. *Journal of Inverse and Ill-Posed Problems, 11*, 191–218.

Rundell, W. (1980). Determination of an unknown non-homogeneous term in a linear partial differential equation from overspecified boundary data. *Applicable Analysis, 10*, 231–242.

Savateev, E. G. (1995). On problems of determining the source function in a parabolic equation. *Journal of Inverse and Ill-Posed Problems, 3*, 83–102.

Skerget, P., & Brebbia, C. A. (1985). Time dependent non-linear potential problems. In C. A. Brebbia (Ed.), *Boundary element research* (pp. 63–86). Berlin: Springer-Verlag.

Twomey, S. (1963). On the numerical solution of Fredholm integral equations of the first kind by the inversion of the linear system produced by quadrature. *Journal of the Association for Computing Machinery, 10*, 97–101.

Xiong, X., Yan, Y., Wang, & J. (2011). A direct numerical method for solving inverse heat source problems. Journal of Physics: Conference Series*, 290*, 012017.

Yan, L., Fu, C. L., & Yang, F. L. (2008). The method of fundamental solutions for the inverse heat source problem. *Engineering Analysis with Boundary Elements, 32*, 216–222.

Yan, L., Yang, F. L., & Fu, C. L. (2009). A meshless method for solving an inverse spacewise-dependent heat source problem. *Journal of Computational Physics, 228*, 123–136.

Yang, L., Dehghan, M., Yua, J.-N., & Luoa, G.-W. (2011). Inverse problem of time-dependent heat sources numerical reconstruction. *Mathematics and Computers in Simulation, 81*, 1656–1672.

Yang, L., Yu, J. N., Luo, G. W., & Deng, Z. C. (2012). Reconstruction of a space and time dependent heat source from finite measurement data. *International Journal of Heat and Mass Transfer, 55*, 6573–6581.